

# Representation of Tropical Mesoscale Convective Systems in a General Circulation Model: Climatology and Response to Global Warming

WENHAO DONG,<sup>a,b</sup> MING ZHAO,<sup>a</sup> YI MING,<sup>a</sup> AND V. RAMASWAMY<sup>a</sup>

<sup>a</sup>NOAA/Geophysical Fluid Dynamics Laboratory, Princeton, New Jersey

<sup>b</sup>Cooperative Programs for the Advancement of Earth System Science, University Corporation for Atmospheric Research, Boulder, Colorado

(Manuscript received 14 July 2020, in final form 2 April 2021)

**ABSTRACT:** The characteristics of tropical mesoscale convective systems (MCSs) simulated with a finer-resolution (~50 km) version of the Geophysical Fluid Dynamics Laboratory (GFDL) AM4 model are evaluated by comparing with a comprehensive long-term observational dataset. It is shown that the model can capture the various aspects of MCSs reasonably well. The simulated spatial distribution of MCSs is broadly in agreement with the observations. This is also true for seasonality and interannual variability over different land and oceanic regions. The simulated MCSs are generally longer-lived, weaker, and larger than observed. Despite these biases, an event-scale analysis suggests that their duration, intensity, and size are strongly correlated. Specifically, longer-lived and stronger events tend to be bigger, which is consistent with the observations. The same model is used to investigate the response of tropical MCSs to global warming using time-slice simulations forced by prescribed sea surface temperatures and sea ice. There is an overall decrease in occurrence frequency, and the reduction over land is more prominent than over ocean.

**KEYWORDS:** Atmosphere; Tropics; Mesoscale systems; Climatology; Climate models

## 1. Introduction

Tropical moist convection is a fundamental process underlying the climate system. Under certain conditions, isolated convective events can aggregate and grow upscale into large clusters or even superclusters by forming mesoscale circulations (Mapes and Houze 1993; Houze 2004, 2018). The resulting mesoscale convective systems (MCSs) represent the largest form of cumulonimbus clouds. Typically, MCSs consist of active convective towers and expansive stratiform regions, a structure that is distinct from scattered or isolated convection. MCSs can be as large as several hundreds of kilometers and last up to more than 24 h (Houze 2004). It has been recognized that MCSs play an important role in redistributing heat, moisture, and momentum (Hartmann et al. 1984; Fritsch et al. 1986; Houze 1989). They are also responsible for producing up to 60% of the total tropical rainfall (Nesbitt et al. 2006; Yuan and Houze 2010; Roca et al. 2014; Houze et al. 2015; Virts and Houze 2015; Tao and Chern 2017). When the environmental conditions are favorable, MCSs can become long-lasting events, producing extreme precipitation (Laing and Fritsch 2000). These durable MCSs are identified to be one of the major causes of flooding over land regions, where they are usually accompanied by strong winds, hail, and even tornadoes (Schumacher and Johnson 2006; Feng et al. 2018). Over the tropical ocean, MCSs occasionally develop into tropical cyclones (Jeong et al. 2016). Thus, MCSs constitute an important

subject as one strives to understand and predict both the tropical mean climate and extreme weather events.

Through a combination of field campaigns, satellite observations, cloud-resolving model (CRM) simulations, and theoretical development, major progresses have been made in recent decades toward better understanding the tropical MCSs (Rotunno et al. 1988; Houze 1989; Moncrieff 1992, 2004, 2010, 2019; Mapes and Houze 1993; Alexander and Cotton 1998; Parker and Johnson 2000; Houze 2004; Moncrieff and Liu 2006; Tao and Chern 2017; Feng et al. 2018). However, the capability (or lack thereof) of general circulation models (GCMs) in simulating MCSs has not been studied in a systematic manner, presumably due to their relatively coarse resolution (hundreds of kilometers). A relevant reference point is that recently developed GCMs with moderately high resolution (tenths of kilometers) have been shown to be capable of simulating tropical cyclone statistics (e.g., Zhao et al. 2009).

Past attempts were made to parameterize the effect of MCSs in GCMs (Donner 1993; Donner et al. 2001; Mapes et al. 2006; Moncrieff et al. 2012; Feng et al. 2018; Moncrieff 2019). The fine-scale cumulus convection embedded in active MCSs requires low-level environmental shear to interact with the cold outflow from convective downdrafts. Yet, these parameterizations are unable to account for the distinct properties of environmental shear, and thus fail to represent the coupling between the cumulus processes and low-level environment realistically (Randall et al. 2016). As a consequence, GCMs, even with parameterized mesoscale convection, have difficulties in simulating the extreme weather events that are closely associated with MCS activities (Moncrieff et al. 2017; Lin et al. 2019). In other words, the inability of GCMs to properly represent MCSs has cast into doubt their skills in simulating and predicting weather and climate extremes. A key structural

 Denotes content that is immediately available upon publication as open access.

Corresponding author: Wenhao Dong, wenhao.dong@noaa.gov

DOI: 10.1175/JCLI-D-20-0535.1

© 2021 American Meteorological Society. For information regarding reuse of this content and general copyright information, consult the [AMS Copyright Policy](#) ([www.ametsoc.org/PUBSReuseLicenses](http://www.ametsoc.org/PUBSReuseLicenses)).

feature of organized moist convection is vertically tilted MCS-like circulations (referred to as slantwise layer overturning) that occur across scales (Moncrieff 2004, 2010). This concept was implemented in the NCAR Community Atmosphere Model by Moncrieff et al. (2017) as a scale-invariant moist convective parameterization. This new paradigm adds key mesoscale heat and momentum transport by cumulus ensembles in sheared environments to traditional cumulus parameterization. For MCSs, by bridging the assumed gap between cumulus and the resolved scales of motion the MCSP (mesoscale convective system parameterization or its generalization multiscale coherent structure parameterization) scheme completes standard cumulus parameterizations.

In this work, we analyze the tropical MCS statistics generated by a  $\sim 50$ -km atmospheric GCM, and apply the same model to explore possible changes of MCS caused by global warming. To our best knowledge, this is the first attempt to assess the performance of a GCM in simulating the key characteristics of tropical MCSs by comparing with a comprehensive long-term observational dataset. The paper is organized as follows. The observational dataset, atmospheric GCM, and MCS detection and tracking algorithm are described in section 2. The present-day tropical MCS simulation and future projection are presented in section 3. A discussion and conclusions are given in section 4.

## 2. Methods

### a. Observational dataset

The Cloud Archive User Service (CLAUS) multisatellite infrared brightness temperature ( $T_b$ ) dataset during 1985–2008 (Hodges et al. 2000) is used to identify and track tropical MCSs (see the detection and tracking algorithm in section 2d). This dataset has a global latitude–longitude spatial resolution of  $1/3^\circ$  at a 3-h time interval, and is quality controlled to remove residual noise and satellite navigation/calibration errors. The CLAUS  $T_b$  dataset is interpolated onto the model grids for a fair comparison. The CERES EBAF Edition 2.8 top-of-the-atmosphere (TOA) fluxes dataset (Loeb et al. 2018) and NOAA interpolated outgoing longwave radiation (OLR) dataset (Liebmann and Smith 1996) are also used for comparison. Besides, the Niño-3.4 index archived at <https://www.esrl.noaa.gov/psd/data/correlation/nina34.data> is used to probe the potential relationship between El Niño–Southern Oscillation (ENSO) and MCSs. Daily precipitation from Global Precipitation Climatology Project (GPCP) dataset (Huffman et al. 2001) during 1997–2008 is used to explore the MCS-related precipitation.

### b. Atmospheric GCM and experimental design

A moderately high-resolution ( $\sim 50$  km) version of the GFDL new atmospheric GCM AM4 [referred to as C192AM4; see details in Zhao (2020)] is used in this study. C192 denotes that there are  $192 \times 192$  grid boxes in each of the six cubed-sphere faces. The same model is also used for GFDL's participation in phase 6 of the Coupled Model Intercomparison Project (CMIP6) HighResMIP project (Haarsma et al. 2016). The original ( $\sim 100$  km) AM4 model (Zhao et al. 2018a,b) is

the atmospheric component of the GFDL coupled physical climate model CM4, GFDL's contribution to CMIP6 (Held et al. 2019). Apart from resolution, the two models differ only in minor details (i.e., time steps, divergence damping, and cloud tunings) (Zhao 2020).

The C192AM4 historical simulations are driven by the observed SST and sea ice conditions, greenhouse gases, and natural and anthropogenic aerosol emissions. We use a three-member ensemble spanning 1950–2014 (referred to as C192AM4-PD) to evaluate the simulated tropical MCSs in the present-day (PD) climate, which is nominally defined as 1985–2008 to coincide with the CLAUS dataset.

In a perturbation experiment (C192AM4-FU), the CMIP5 multimodel mean SST and sea ice anomalies in the RCP8.5 future (FU) scenario are superposed on the PD climatology. The resulting simulation covers the period of 2015–50; years 2027–50 are compared with the PD simulation, which is of the same duration (24 years), to assess the response of tropical MCSs.

To discern the relative roles of mean SST and SST pattern in affecting the response, we also examine a pair of idealized experiments, both of which are integrated for 31 years with the first year as spinup. The control (CL) simulation (C192AM4-CL) is forced with the 2010 climatological SST, sea ice, and radiative forcings, while the perturbation simulation is identical except for a uniform 4-K increase in SST (C192AM4-4K). Note that the global mean surface temperature differs by 1.2 K between C192AM4-FU and C192AM4-PD (the former minus the latter, as is the convention throughout the paper), and by 4.5 K between C192AM4-4K and C192AM4-CL. The projected changes in MCSs are normalized by their respective global mean temperature changes.

### c. Conversion from OLR to $T_b$

The brightness temperature  $T_b$  is not simulated directly by the model, but can be inferred rather accurately from outgoing longwave radiation (OLR) by the following:

$$\begin{cases} T_F = T_b(a + bT_b) \\ \text{OLR} = \sigma T_F^4 \end{cases},$$

where  $T_F$  is the flux equivalent brightness temperature,  $\sigma = 5.67 \times 10^{-8} \text{ W m}^{-2} \text{ K}^{-4}$  is the Stefan–Boltzmann constant, and  $a$  and  $b$  are empirical coefficients based on regression (Ohring et al. 1984). We set  $a$  at 1.228 and  $b$  at  $-1.106 \times 10^{-3} \text{ K}^{-1}$  as in Ellingson and Ferraro (1983). Similar relationships have been used to calculate OLR from the AVHRR-retrieved brightness temperature (Abel and Gruber 1979). Although the coefficients  $a$  and  $b$  vary slightly with different regression equations as discussed in Ohring et al. (1984), the results reported here are not sensitive to these subtle changes.

The model-simulated mean  $T_b$  is compared with the CLAUS-observed counterpart in Fig. 1. The spatial distributions are generally in good agreement, with the values over the vast subsiding regions higher than over the west Pacific warm pool (WPWP). The centered pattern correlation is 0.93 ( $P < 0.001$ ) when both datasets are interpolated onto the same  $1^\circ \times 1^\circ$  grids. The difference plot reveals that the modeled  $T_b$  are

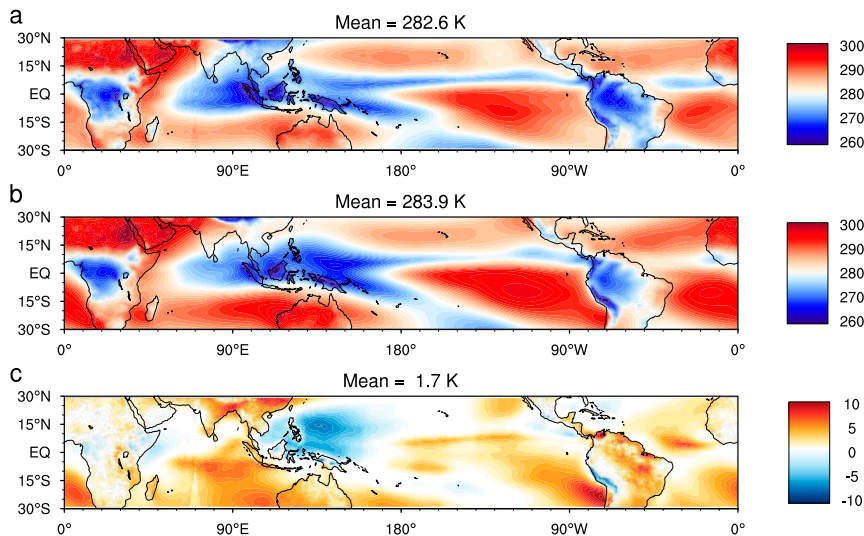


FIG. 1. Spatial distribution of time-average brightness temperature (K) from (a) CLAUS and (b) C192AM4-PD for 1985–2008, and (c) the difference of (b) minus (a).

overestimated to varying degrees almost everywhere in the tropics, with the notable exception of the eastern part of WPWP.

#### d. MCS detection and tracking algorithm

We adopt the automated MCS detection and tracking algorithm developed by Huang et al. (2018). This two-step algorithm is designed to identify MCSs based on a  $T_b$  threshold and a minimum area coverage threshold, which are set at 233 K and 5000 km<sup>2</sup>, respectively, in this study. These threshold values have been used extensively in previous studies (Williams and Houze 1987; Pope et al. 2009; Goyens et al. 2012; Fiolleau and Roca 2013). After the initial identification, a tracking procedure is performed to link each MCS. Conventional area-overlapping tracking assumes that the candidate systems in consecutive timeframes belong to the same MCS if there is sufficient overlapping in area (15% in this study). This is problematic for small or fast-moving MCSs since there may not be overlapping between two timeframes. In contrast, the algorithm used here invokes a Kalman filter approach, which proves to be an optimal estimator for the movement of potential MCSs (Xing et al. 2009). The reader is referred to Huang et al. (2018) for more detail about the algorithm and comparison with other algorithms. All MCSs identified and tracked over the tropics (30°S–30°N) are recorded in sequence for each month, but the records for the first and last months are discarded to ensure complete life cycles.

### 3. Results

#### a. Spatial distribution

The CLAUS-based time-average track density of tropical MCSs is illustrated in Fig. 2a. The spatial distribution bears a strong resemblance to that of tropical precipitation. This is understandable as MCSs produce more than half of the total

tropical precipitation, as discussed in the introduction. Over ocean, frequent occurrences of MCSs are seen over the intertropical convergence zone (ITCZ) and South Pacific convergence zone (SPCZ). The northern Indian Ocean is another region with significant presence of MCSs. Africa and South America (mainly the Amazon) are two major land regions characteristic of intensive MCS activities. The Maritime Continent is of special interest. Although it is debatable whether this region is continental or maritime (Houze et al. 2015), it clearly has more frequent MCSs than the surrounding oceanic surface. These three regions (Africa, South America, and the Maritime Continent) have long been known as the key regions of deep convection and associated diabatic heating driving the tropical circulation (Webster 1974). The spatial pattern present here is broadly consistent with previous studies based on a variety of observational datasets (Yuan and Houze 2010; Houze et al. 2015; Moncrieff et al. 2017).

The C192AM4-PD simulation captures the observed spatial distribution of tropical MCSs reasonably well, with a centered pattern correlation of 0.87 ( $P < 0.001$ ) (Fig. 2b). All the regions with active MCSs discussed above feature prominently in the simulation. An inspection of the difference plot (Fig. 2c) reveals that the simulated distribution of MCSs over the ITCZ and SPCZ is not as compacted as observed. As a result, the model simulates fewer MCSs over these convergence zones, but tends to overestimate them elsewhere over ocean. The biases over land are not as structured, but there is a tendency to underestimate over the Amazon and Maritime Continent and to overestimate over Africa. Furthermore, the linkage between orography and MCS occurrence, albeit strong in the observations, is exaggerated in the model simulation (e.g., over the windward slopes of the Himalayas and Andes).

The track density of MCSs depends on both genesis and duration. We shall focus on genesis here and discuss duration in section 3c. To facilitate regional analysis, the tropics are divided roughly into eight regions (as delineated by the rectangles

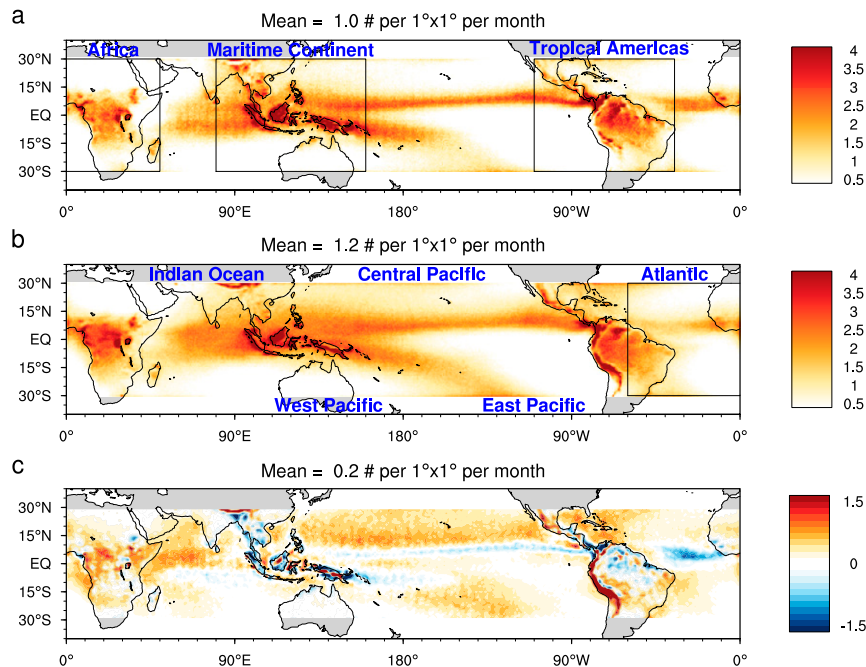


FIG. 2. Track density of tropical MCSs (number per  $1^{\circ} \times 1^{\circ}$  per month) based on (a) CLAU S and (b) C192AM4-PD for 1985–2008, and (c) the difference of (b) minus (a). Rectangles in (a) and (b) denote the different regions used for the subsequent analysis.

in Fig. 2). Note that there are three regions over the Pacific (i.e., west, central, and east Pacific). The rationale is that the different sectors of the Pacific basin were reported to show distinct MCS variability (Dong et al. 2020). Oceanic grids are masked out for land analysis, and vice versa. Table 1 lists the observed annual mean genesis counts for different regions and the corresponding model biases. (Note that the spread among the three ensemble members is within a few percentage points.) The model underestimates range from  $-21\%$  to  $16\%$ , with the largest bias over the Maritime Continent (Table 1), and the tropical mean bias is  $-0.4\%$ .

#### b. Seasonality and interannual variability

Figure 3 compares the simulated seasonal cycles of tropical MCSs with the observations over the analysis regions. The annual means are removed for this analysis. Overall, the model

shows considerable skills in capturing the amplitudes and phases of the observed seasonal cycles. The positive correlation coefficients ( $R$ ) are statistically significant for six out of the eight regions (Table 1). A notable exception is the Indian Ocean, where the model-simulated MCSs are most active in the South Asian monsoon season (June–September), out of phase with the observed seasonal cycle peaking in October–January. This is presumably because atmosphere models forced with prescribed SSTs are unable to capture effects of the strong air–sea coupling over the Indian Ocean (Lau and Nath 2003).

Figure 4 concerns the interannual variability of tropical MCS activities. The model performance varies between land and oceanic regions. Despite its ability in reproducing the observed interannual variability for all oceanic regions and the Maritime Continent, the model shows no skill over Africa and

TABLE 1. Observed annual mean genesis counts of tropical MCSs and model biases (%), and the correlation coefficients between the observed and simulated MCS frequencies at seasonal and interannual time scales (boldface denotes statistical significance at the 95% confidence interval) for different regions.

Region	Genesis		Correlation	
	Observed	Model bias	Seasonal	Interannual
Africa	5085	6.8%	<b>0.87</b>	0.26
Maritime Continent	5184	$-21.0\%$	<b>0.97</b>	<b>0.72</b>
Tropical Americas	6507	$-5.1\%$	<b>0.89</b>	0.49
Indian Ocean	5341	$-2.3\%$	$-0.66$	<b>0.52</b>
West Pacific	5755	$-6.1\%$	<b>0.86</b>	<b>0.93</b>
Central Pacific	7986	3.3%	<b>0.71</b>	<b>0.64</b>
East Pacific	4312	16.2%	0.51	<b>0.81</b>
Atlantic	3309	4.8%	<b>0.91</b>	<b>0.58</b>

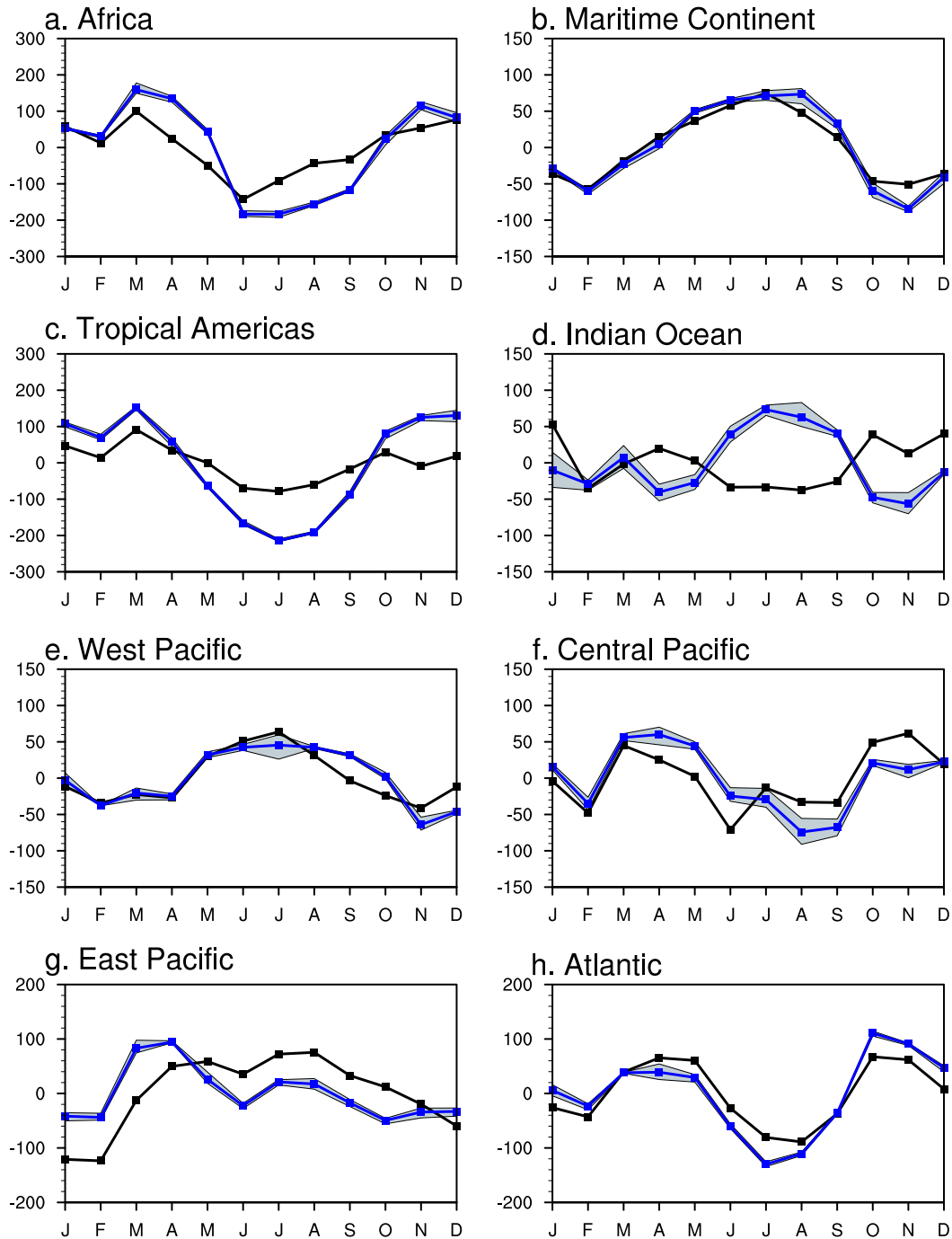


FIG. 3. Observed (CLAUS; black) and simulated (C192AM4-PD; blue) seasonal cycles of tropical MCS frequency (number per month) for each region. The respective annual means are subtracted. The light blue shading denotes the spread among the three ensemble members.

the tropical Americas (Table 1). This implies that the interannual variability over tropical land is not driven, at least to zeroth order, by the oceanic conditions, and may involve complex land processes and atmosphere–land interactions. On a related note, the ensemble mean is invariably better than any individual ensemble member in reproducing the observed

interannual variability for every region. This is consistent with Zhao et al. (2009) in the context of Atlantic hurricane counts, suggesting that the genesis frequency of tropical MCSs may have a large component that is predictable from SSTs.

The interannual variability of MCSs over west Pacific is out of phase with that over the east Pacific. This is true for both the

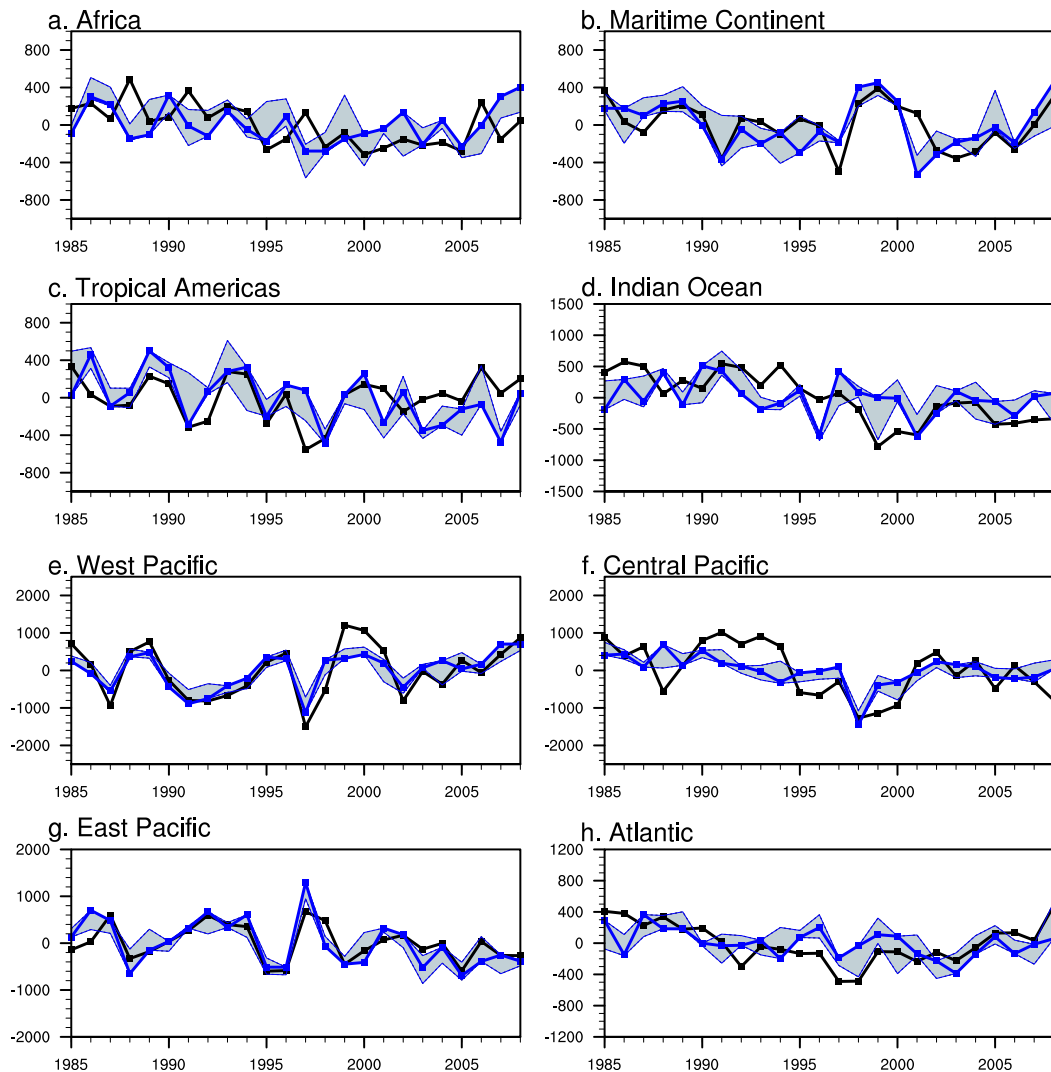


FIG. 4. Observed (CLAUS; black) and simulated (C192AM4-PD; blue) interannual variations of tropical MCS for each region. The respective 1985–2008 means are subtracted. The light blue shading denotes the spread among the three ensemble members.

observations ( $R = -0.80$ ,  $P < 0.01$ ) and the simulations ( $R = -0.71$ ,  $P < 0.01$ ). The seesaw pattern between these two regions may be indicative of the significant role of underlying SST patterns, especially that associated with ENSO events, in shaping the spatial distribution of MCSs over the Pacific. One can support this argument by correlating the observed Niño-3.4 index with the observed MCS counts over these two regions. The correlation coefficient is  $-0.93$  over the west Pacific and  $0.72$  over the east Pacific, both of which are statistically significant at the 99.9% confidence interval.

### c. Duration, intensity, and size

A key characteristic of MCSs, duration or lifetime, is tightly linked to rainfall production. Long-lived MCSs are often accompanied by large accumulative precipitation, and may lead to flood events. The spatial distribution of MCS duration is

shown in Fig. 5. The model generally captures the pattern of the observed MCS duration but on average overestimates the lifetime by two timeframes ( $\sim 6$  h). The overestimation is especially prominent over the Indian Ocean and western Pacific. These long-lived oceanic MCS may be related to the overproduced tropical cyclones in the model simulations. We then calculate the normalized histograms of MCS duration with a 3-h interval for all regions, and find that the distribution patterns are quite similar. For brevity, only the results for two regions, namely Africa (representative of land) and the west Pacific (representative of ocean) are presented in Fig. 6. The model is able to reproduce the observed monotonic decrease of probability with duration (Pope et al. 2008; Roca et al. 2017), but is biased toward longer lifetimes. In particular, the observed cumulative probability of those events lasting less than 12 h is 66% for Africa and 60% for the west Pacific as compared

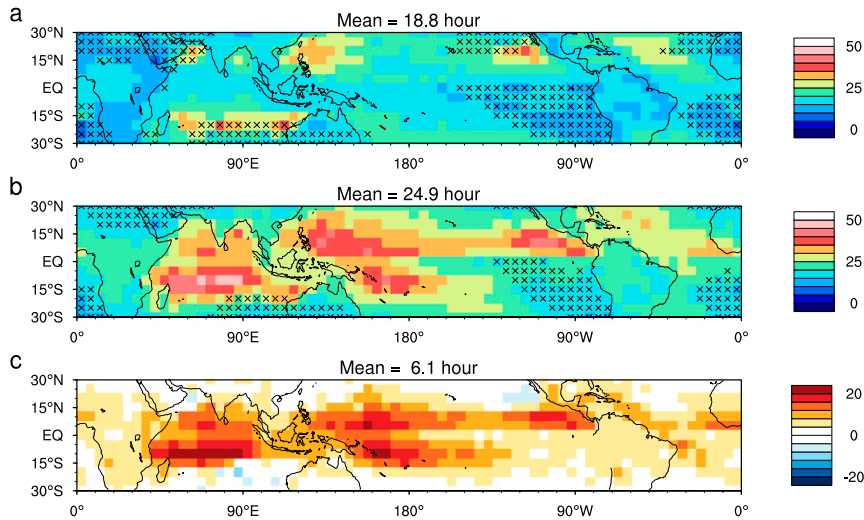


FIG. 5. Spatial distribution of MCS duration (h) from (a) CLAUS and (b) C192AM4-PD for 1985–2008, and (c) the difference of (b) minus (a). Crosses indicate where the sample size is smaller than 100.

to 53% for Africa and 48% for the west Pacific in the model. We also probe the probability of long-lasting MCSs, defined as those longer than 24 h. They account for 14% of the MCSs over Africa and 17% over the west Pacific in the observations, whereas the model overestimates them by a factor of 2 (23% and 28%, respectively). The observations also hint at the MCSs over ocean lasting long than those over land; the mean (median) duration is 12.3 (9.0) hours for Africa, which is shorter than 14.4 (12.0) hours for the west Pacific. This land–sea contrast is borne out in the simulation; the simulated mean (median) duration is 17.1 (12.0) hours for Africa and 21.0 (15.0) hours for the west Pacific.

Unlike tropical cyclone, there is no commonly adopted definition of intensity for MCSs. Previous studies used a wide variety of metrics such as horizontal wind, vertical wind shear, temperature, and moisture (LeMone and Zipser 1980; McCaul et al. 2005; Takemi 2010). This study uses  $T_b$  averaged over all the grid points occupied by a MCS and its lifetime as a proxy of intensity. The model captures the spatial distribution of  $T_b$ , but overestimates it by 1.5 K on average (Fig. 7). This is in line with the expectation that a moderately high-resolution model like the one used here cannot resolve the full strength of MCSs. Such an underestimation is also evident in the probability density distribution of intensity (Fig. 8). The simulations are

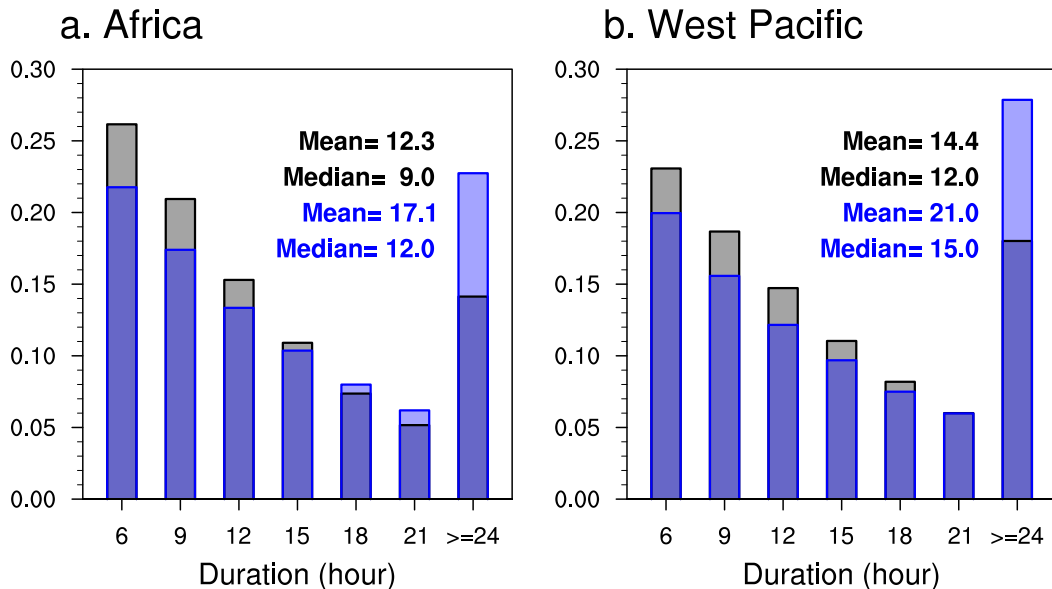


FIG. 6. Observed (CLAUS; black) and simulated (C192AM4-PD; blue) normalized histograms of the duration of tropical MCS for (a) Africa and (b) west Pacific. The mean and median (h) are listed.

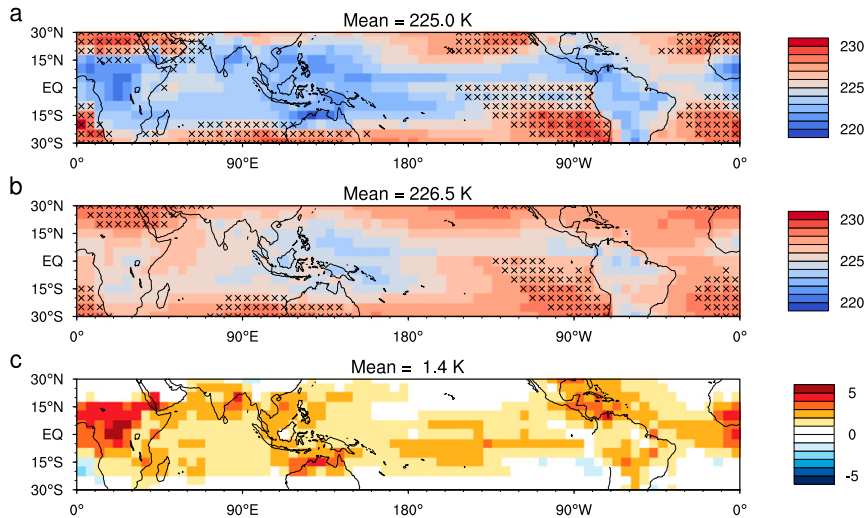


FIG. 7. Spatial distribution of MCS intensity (K) from (a) CLAU and (b) C192AM4-PD for 1985–2008, and (c) the difference of (b) minus (a). Crosses indicate where the sample size is smaller than 100.

more skewed than the observations toward higher  $T_b$  values. This is particularly true for Africa, where the simulated distribution is substantially narrower than observed.

The identified MCSs in the observations and simulations are averaged into the same  $5^\circ \times 5^\circ$  grid boxes before computing sizes averaged during lifetime. This coarse graining procedure is designed to optimize statistical robustness by balancing the competing needs to reduce noise through averaging and to retain enough samples. Comparatively large MCSs are observed over central Africa, the Bay of Bengal, the west Pacific, and South America (Fig. 9). This overall pattern is borne out in the model simulation, albeit with large overestimation over the

west Pacific. The probability density distributions of MCS size over Africa and the west Pacific are shown in Fig. 10. Both regions are characterized by a distinct peak at around 10 000–20 000 km<sup>2</sup>, accompanied by a long tail. About 62% of the observed MCS are smaller than 50 000 km<sup>2</sup>. The model reproduces the gamma-shaped distributions. The simulated mean and median sizes are comparable to the observations over Africa, but are nearly twice over the west Pacific. The cumulative probability of MCSs smaller than 50 000 km<sup>2</sup> is 58% in the simulation.

Although the three attributes are evaluated separately in the above analysis, it is widely known that they are tightly

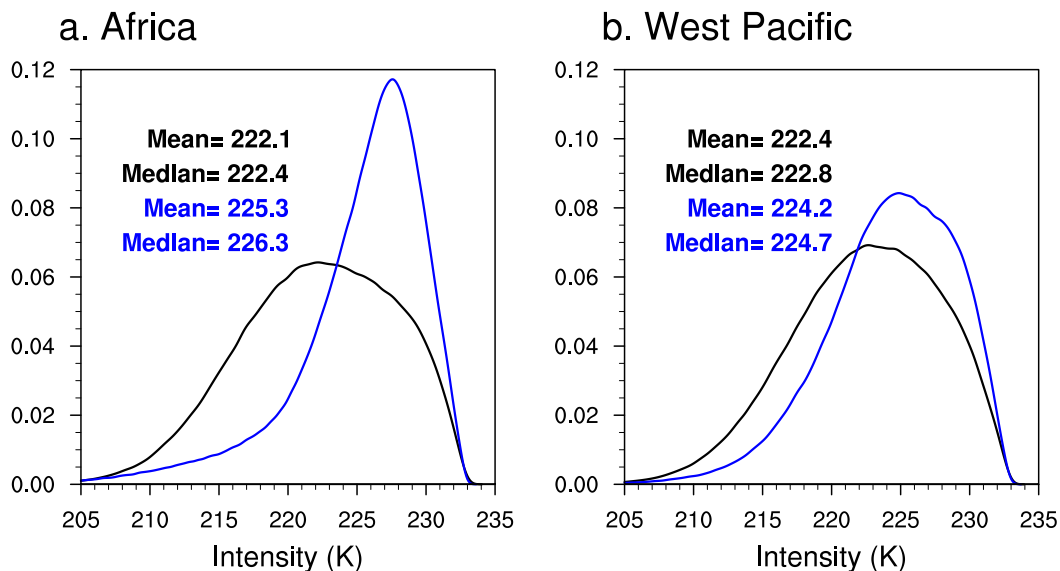


FIG. 8. Observed (CLAUS; black) and simulated (C192AM4-PD; blue) probability density distribution of MCS intensity (K) for (a) Africa and (b) the west Pacific. The mean and median (K) are listed.

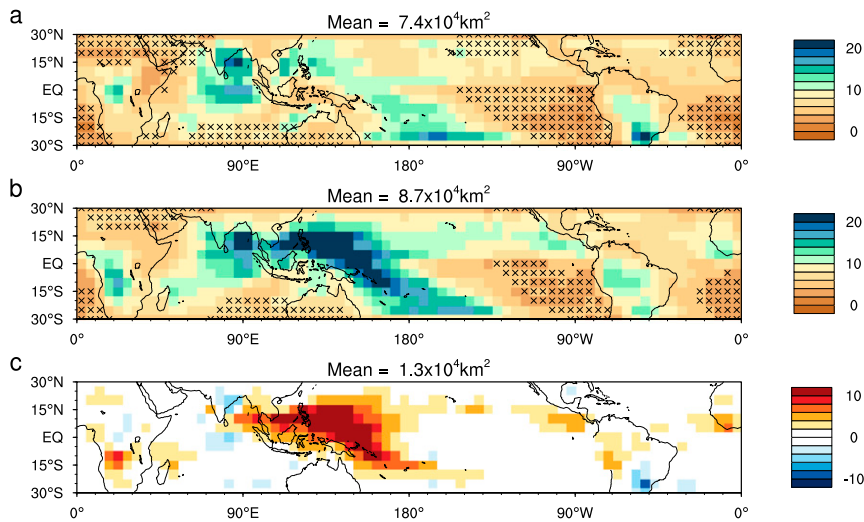


FIG. 9. As in Fig. 7, but for MCS size ( $10^4 \text{ km}^2$ ).

correlated. Here, we examine how MCS size or intensity varies with duration. Note that the size and intensity of an individual event are averaged over its entire life cycle, and the results are qualitatively similar if the maximum size or intensity is used instead. The duration–size relationship is illustrated in Fig. 11. Two metrics, namely the mean and the 95th percentile sizes of the events falling into a specific duration bin, are used to evaluate the dependence of MCS size on duration. The 95th percentile size enables one to examine the behaviors of comparatively large MCSs. The observations show a strong correlation between MCS duration and size; longer-lived MCSs are generally larger. This is consistent with the study by Machado et al. (1998), in which a nearly linear relationship between the average MCS radius and its life cycle was found over the Americas. The normalized rate of change is 4.4% increase in

size per 1-h increase in duration ( $P < 0.001$ ) over Africa, and 4.7% over the western Pacific ( $P < 0.001$ ). The numbers remain almost unchanged for the 95th percentile size. The model performance diverges over the two regions, with an excellent agreement with the observations over Africa. The large positive bias in MCS size over west Pacific makes it difficult to compare directly with the observations, especially for the 95th percentile size. The strong duration–size relationship is clearly present in the simulation, and the normalized rates of change are within a factor of 2. Overall, our results indicate that the dependence of MCS size on duration is robust throughout the tropics at an average rate of about 4% increase in size per 1-h increase in duration.

The same method enables us to explore the relationship between MCS intensity and size. The brightness temperature

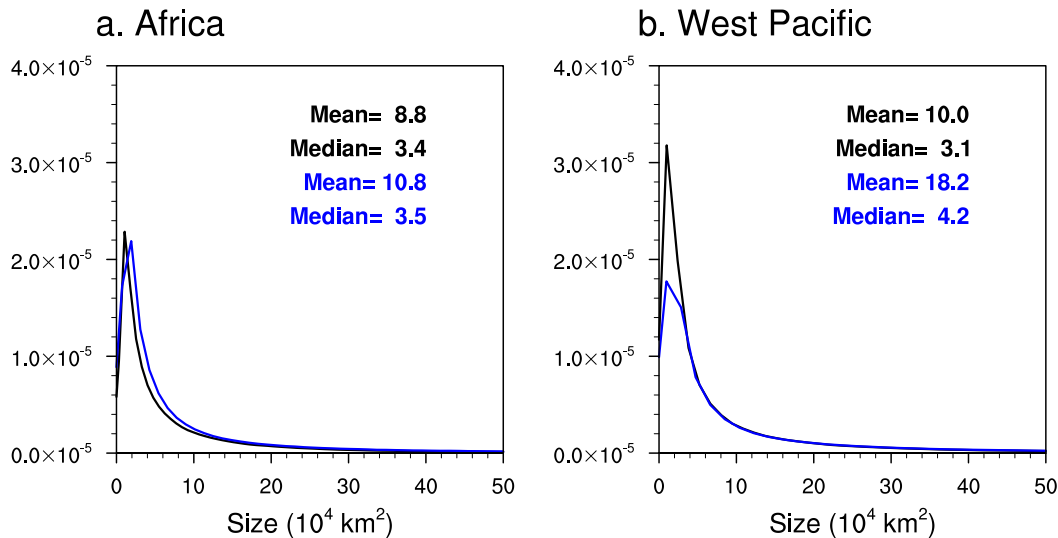


FIG. 10. As in Fig. 8, but for MCS size.

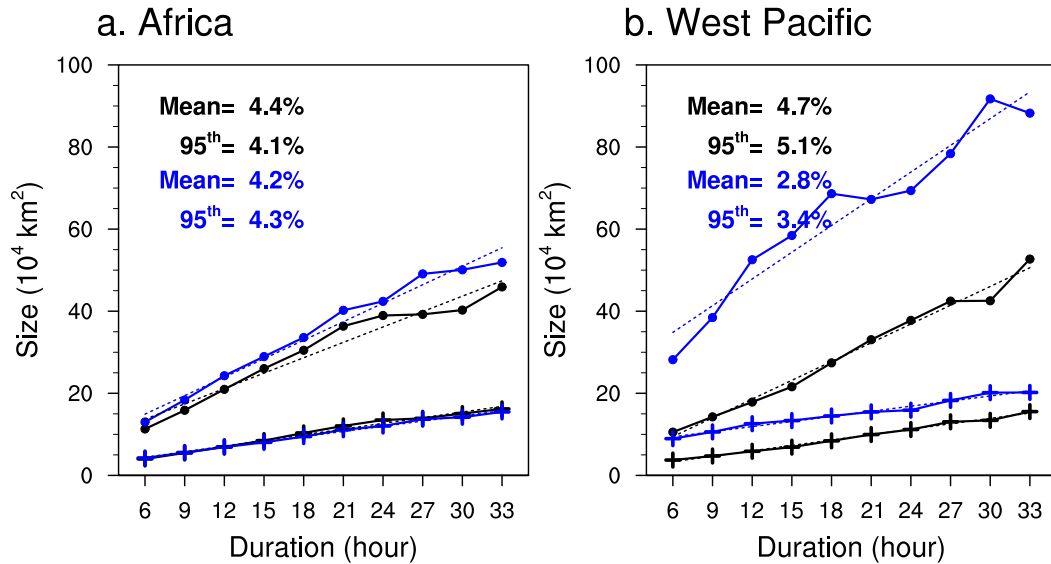


FIG. 11. Relationship between MCS duration (h) and size ( $10^4 \text{ km}^2$ ) for (a) Africa and (b) the west Pacific. Individual events are binned based on duration with an interval of 3 h. The lines with cross markers are for the mean size, and the lines with solid dots are for the 95th percentile size. The dashed lines are the best linear fits. The normalized rates of change (% per hour) are listed for the mean and 95th percentile size.

of most MCS spans over a range of 213–233 K in both the observation and model simulations, which is divided into 10 evenly placed bins. A significant negative correlation between brightness temperature and size holds for the observations and simulations alike, meaning that stronger MCSs (lower brightness temperature) tend to be larger (Fig. 12). The observed rate of change is 13.0% decrease in size per 1 K increase in intensity over Africa, and 16.0% over the west Pacific. The values are almost the same for the 95th percentile size. Both metrics are followed closely by the model.

#### d. Future projection

It has been shown that C192AM4 is skillful at simulating the observed main characteristics of tropical MCSs, lending credence to its utility in studying the response of MCS statistics to global warming and implications for weather extremes. Figure 13 shows the projected track density of tropical MCSs based on the C192AM4-FU simulation and its difference from C192AM4-PD (Fig. 2b). Although the spatial structure remains the same in the warming case, there are distinct changes on the regional scale. The occurrences over tropical land such

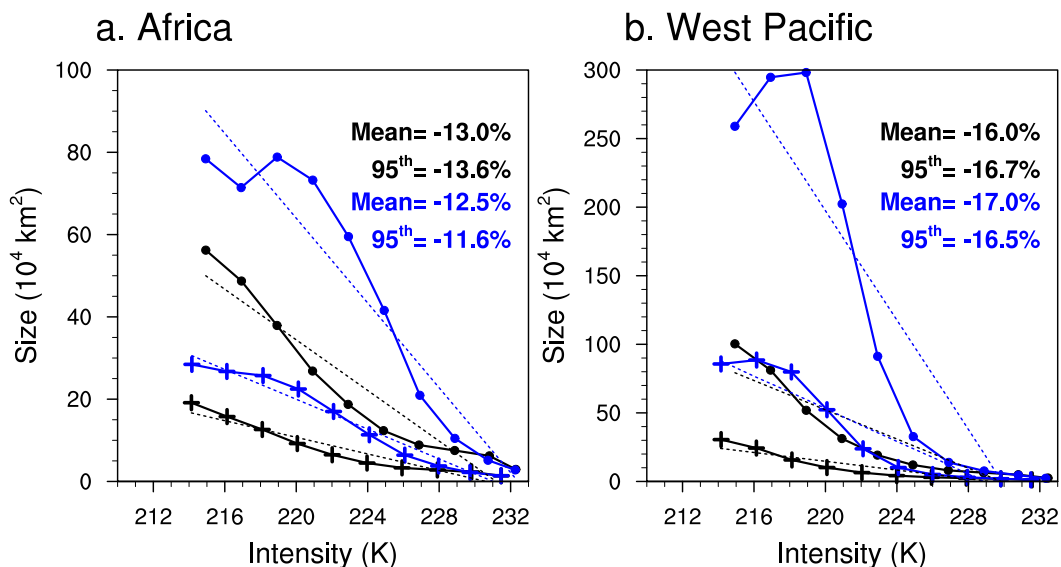


FIG. 12. As in Fig. 11, but for the relationship between MCS intensity (K) and size ( $10^4 \text{ km}^2$ ).

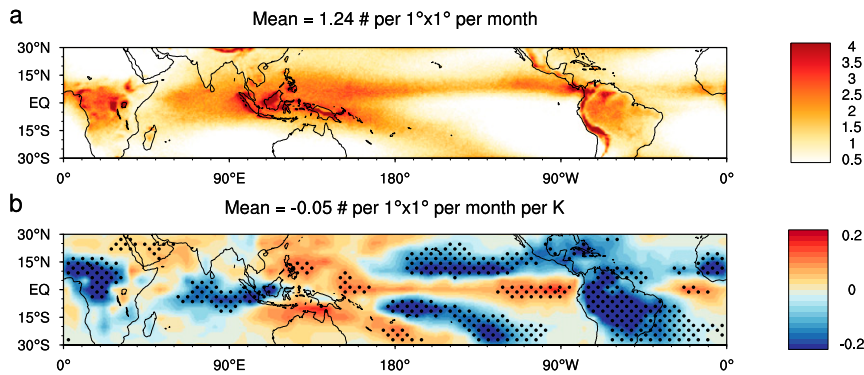


FIG. 13. (a) Track density of tropical MCSs (number per  $1^\circ \times 1^\circ$  area per month) based on C192AM4-FU. (b) The difference (number per  $1^\circ \times 1^\circ$  area per month per kelvin) between C192AM4-FU and C192AM4-PD (Fig. 2b) normalized by the global mean temperature change (the former minus the latter). Black dots in (b) indicate where the results are statistically significant at the 95% confidence level based on a 1000-fold resample bootstrapping method.

as Africa and the tropical Americas are projected to decrease. In comparison, the signals over ocean are less robust. We also contrast the C192AM4-4K and C192AM4-CL simulations to help rationalize the effects of uniform versus spatially varying warming. As illustrated in Fig. 14, the idealized uniform warming case shares many similarities with the realistic warming case. Most notably, the MCS occurrence is reduced almost everywhere over tropical land in the uniform warming case, with significant implications for the continental hydrological extremes.

Overall, the total number of tropical MCSs decreases by 3.0% per 1 K warming in C192AM4-FU. The decrease is more prominent over land (5.6%) than over ocean (1.6%). The uniform 4-K warming experiment yields similar results. The reduction in MCS number is 1.6% per kelvin for the entire tropics (5.4% over land and 0.5% over ocean), and is primarily due to the decrease in genesis number. Any change in MCS duration, intensity, or size is small in both pairs of experiments. The projected reduction in MCS number in the warming scenario could be associated with the decreased convective mass

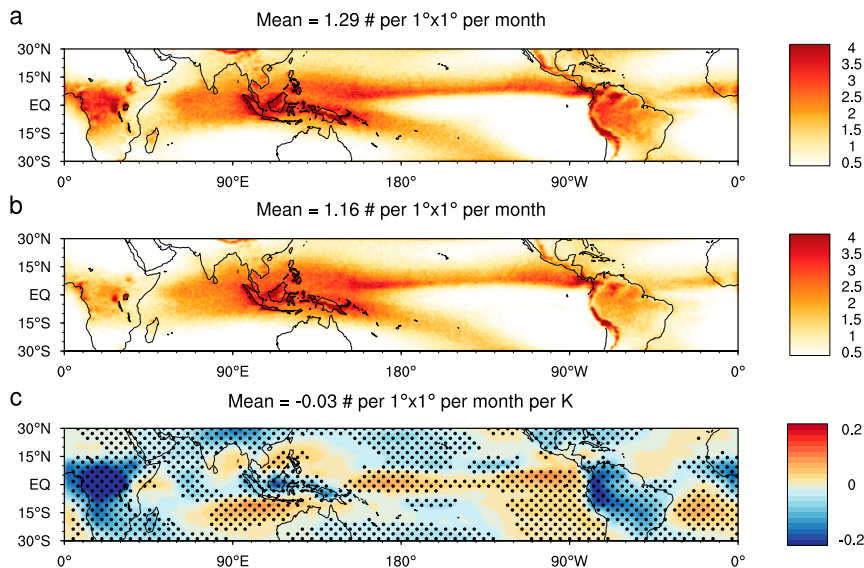


FIG. 14. Track density of tropical MCSs (number per  $1^\circ \times 1^\circ$  area per month) based on (a) C192AM4-CL and (b) C192AM4-4K (Fig. 2b), and (c) the difference of (b) minus (a) normalized by the global mean temperature change. Black dots in (b) indicate where the results are statistically significant at the 95% confidence level based on a 1000-fold resample bootstrapping method.

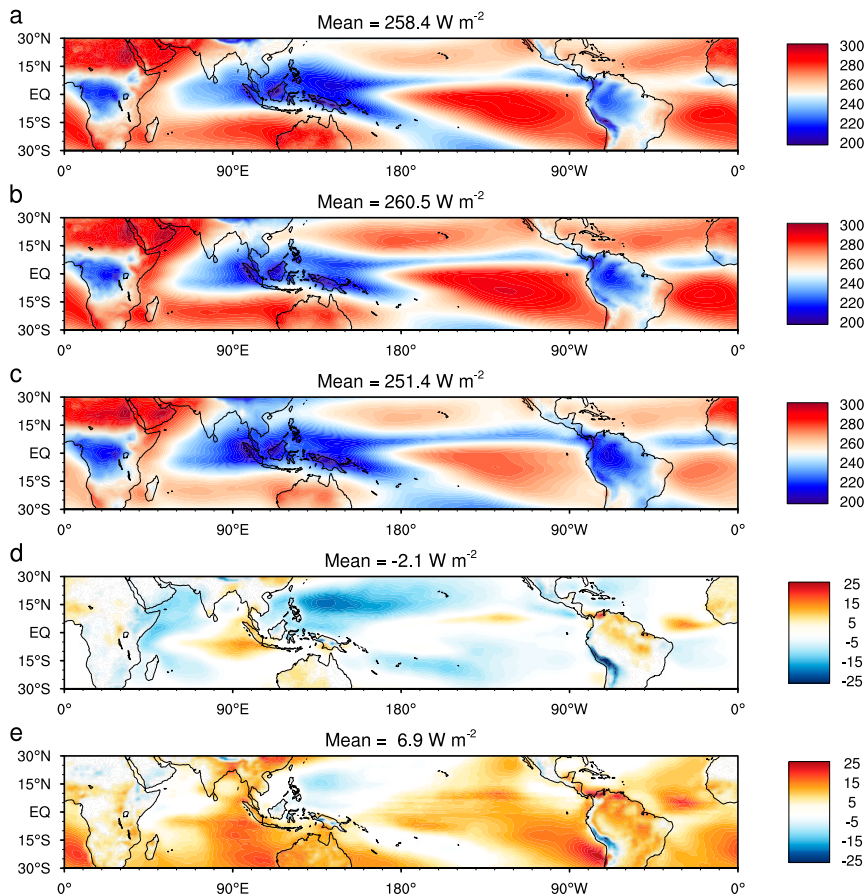


FIG. 15. Spatial distribution of time-average OLR ( $\text{W m}^{-2}$ ) based on (a) C192AM4-PD simulations, (b) CERES EBAF OLR, and (c) NOAA Interpolated OLR during the overlapping period of 2000–14. (d), (e) The differences of (a) minus (b) and (a) minus (c), respectively.

flux (Held and Soden 2006), while more needs to be done to better understand the disparity between land and ocean.

#### 4. Discussion and conclusions

To examine the potential impacts of threshold choices on identifying tropical MCSs, we perform three sensitivity tests using different thresholds, namely a smaller  $T_b$  (228 K), a larger minimum area coverage (10 000 km<sup>2</sup>), and a larger overlapping fraction (25%), as in Huang et al. (2018). They are compared with the results based on the default parameters (i.e., brightness temperature of 233 K, minimum area coverage of 5000 km<sup>2</sup>, and overlapping fraction of 15%). It is found that the spatial distribution of tropical MCSs remains virtually unchanged (not shown). The total number of identified MCSs is most sensitive to the choice of minimum area threshold. For example, using a minimum area threshold of 10 000 km<sup>2</sup> results in a reduction of 10% in the total number for the observations. This is also true to similar extents for all simulations. The differences are nonnegligible, but do not change the main conclusions.

The simulated OLR in C192AM4-PD is compared with the CERES EBAF OLR as well as the NOAA Interpolated OLR for the overlapping period of 2000–14 (Fig. 15). The simulated tropical-mean OLR is  $258.4 \text{ W m}^{-2}$ , which is close to CERES EBAF ( $260.5 \text{ W m}^{-2}$ ). This is understandable as the model's radiative balance was tuned specifically against CERES. Yet, CERES is substantially larger than the NOAA interpolated OLR ( $251.4 \text{ W m}^{-2}$ ). There is also appreciable difference between AVHRR and CERES. Although CERES has been validated extensively by comparing with ground-based measurements over land and ocean, uncertainties may still persist. Although an objective assessment of the different observational datasets is beyond the scope of this study, we stress that the underestimation of the total MCS genesis number may be at least partly due to the model-simulated OLR being too high. The underestimation of MCSs intensity, especially over tropical land, may be an indication of the model's deficiency in simulating deep convections. In other words, the simulated MCSs are less penetrative than observed.

Besides model resolutions, convective parameterizations also play a central role in simulating tropical transients,

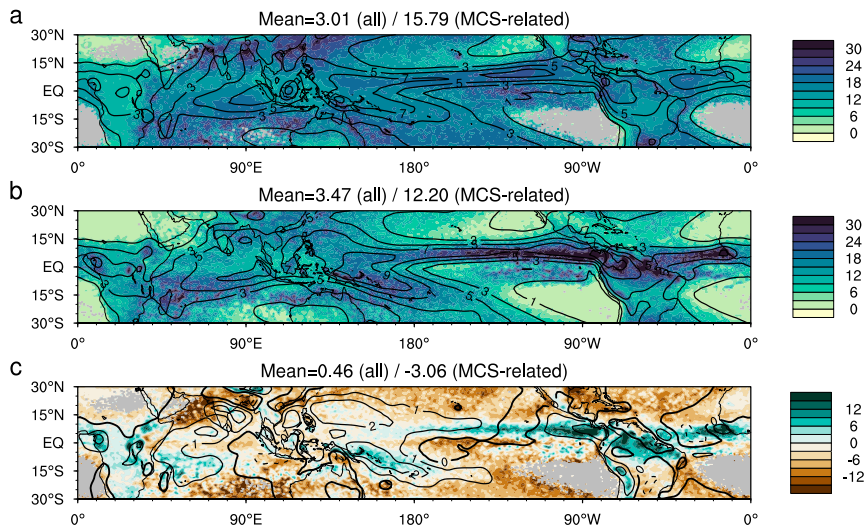


FIG. 16. Tropical mean precipitation (contour;  $\text{mm day}^{-1}$ ) and precipitation associated with MCSs (shading;  $\text{mm day}^{-1}$ ) based on (a) GPCP and (b) C192AM4 for 1997–2008, and (c) the difference of (b) minus (a).

including MCSs. The deep convection scheme used in AM4 is less penetrative than those in its predecessors (AM2 and AM3) mainly due to more efficient lateral mixing (Zhao et al. 2018a). As a result, the large-scale fraction of the total tropical precipitation, a quantitative measure of how active a cumulus parameterization is, in AM4 ( $\sim 30\%$ ) is substantially higher. This generally favors more active tropical transients. Note that a 60-km grid Weather Research and Forecasting (WRF) Model, equipped with a standard Betts–Miller convective parameterization and an elementary mesoscale parameterization, also produces extensive large-scale or resolved rainfall (Moncrieff and Liu 2006). The current study, however, does not directly address the relative importance of model resolutions versus convective parameterizations in simulating the tropical MCSs.

In summary, we use a moderately high-resolution AM4 model (C192AM4) to study the response of tropical MCSs to global warming. By comparing with the CLAUS observational dataset during 1985–2008, the historical simulation is shown to capture the key tropical MCS feature including the spatial distribution, seasonality, interannual variability, duration, intensity, and size. Although the total number of tropical MCSs is well simulated (the mean bias is less than 1%), the model overestimates MCS duration and size over west Pacific. Nonetheless, it can reproduce the strong relationship between duration (intensity) and size. The two sets of perturbations experiments (realistic and uniform warming) give rise to similar features in MCS change, the most prominent one being a reduction in the occurrence of MCSs over tropical land (5.7% and 5.4%, respectively). It is important to assess the robustness of these results in fully coupled models as the current work is hindered by the lack of air–sea interaction in the AMIP-type simulations.

Much remains to be understood about the effects of MCSs across scales, including how they operate in state-of-the-art

GCMs. As highlighted by Moncrieff et al. (2017), realistic representation of the atmospheric water cycle, a major climate science challenge, involves complex and nonlinear interactions from the microscale to global scale. Realistic surface rainfall in GCMs is crucial for coupling the atmosphere to land and ocean surface with implications for society, ecology, and beyond. As a first step, we analyze the MCS-related precipitation in both the observation and C192AM4 simulations. Figure 16 shows that the observed precipitation associated with MCSs largely resembles its long-term mean pattern, but with a much larger magnitude. Both the mean pattern and the portion related to the MCSs are well captured by the model. It should be pointed out that these results, based on daily records, may be biased low as coarse temporal resolutions tend to smooth out the precipitation maxima associated with MCSs.

*Acknowledgments.* The authors thank Pu Lin and Xing Huang for useful discussion on the implementation of the MCS tracking algorithm, and thank Kun Gao, Tsung-Lin Hsieh, and Leo Donner for commenting on earlier versions of this paper. Addressing the constructive comments by Dr. Mitchell Moncrieff and two anonymous reviewers has greatly improved the paper. This research from the Geophysical Fluid Dynamics Laboratory is supported by NOAA’s Science Collaboration Program and administered by UCAR’s Cooperative Programs for the Advancement of Earth System Science (CPAESS) under awards NA16NWS4620043 and NA18NWS4620043B.

## REFERENCES

- Abel, P., and A. Gruber, 1979: An improved model for the calculation of longwave flux at  $11\ \mu\text{m}$ . NOAA Tech. Rep. NWS 106, NTIS PB80-119431, 24 pp.
- Alexander, G. D., and W. R. Cotton, 1998: The use of cloud-resolving simulations of mesoscale convective systems to build a mesoscale parameterization scheme. *J. Atmos. Sci.*, **55**,

- 2137–2161, [https://doi.org/10.1175/1520-0469\(1998\)055<2137:TUOCRS>2.0.CO;2](https://doi.org/10.1175/1520-0469(1998)055<2137:TUOCRS>2.0.CO;2).
- Dong, W. H., Y. L. Lin, M. H. Zhang, and X. M. Huang, 2020: Footprint of tropical mesoscale convective system variability on stratospheric water vapor. *Geophys. Res. Lett.*, **47**, e2019GL086320, <https://doi.org/10.1029/2019GL086320>.
- Donner, L. J., 1993: A cumulus parameterization including mass fluxes, vertical momentum dynamics, and mesoscale effects. *J. Atmos. Sci.*, **50**, 889–906, [https://doi.org/10.1175/1520-0469\(1993\)050<0889:ACPIMF>2.0.CO;2](https://doi.org/10.1175/1520-0469(1993)050<0889:ACPIMF>2.0.CO;2).
- , C. J. Seman, R. S. Hemler, and S. M. Fan, 2001: A cumulus parameterization including mass fluxes, convective vertical velocities, and mesoscale effects: Thermodynamic and hydrological aspects in a general circulation model. *J. Climate*, **14**, 3444–3463, [https://doi.org/10.1175/1520-0442\(2001\)014<3444:ACPIMF>2.0.CO;2](https://doi.org/10.1175/1520-0442(2001)014<3444:ACPIMF>2.0.CO;2).
- Ellingson, R. G., and R. R. Ferraro, 1983: An examination of a technique for estimating the longwave radiation budget from satellite radiance observations. *J. Climate Appl. Meteor.*, **22**, 1416–1423, [https://doi.org/10.1175/1520-0450\(1983\)022<1416:AEOATF>2.0.CO;2](https://doi.org/10.1175/1520-0450(1983)022<1416:AEOATF>2.0.CO;2).
- Feng, Z., L. R. Leung, R. A. Houze Jr., S. Hagos, J. Hardin, Q. Yang, B. Han, and J. Fan, 2018: Structure and evolution of mesoscale convective systems: Sensitivity to cloud microphysics in convection-permitting simulations over the United States. *J. Adv. Model. Earth Syst.*, **10**, 1470–1494, <https://doi.org/10.1029/2018MS001305>.
- Folleau, T., and R. Roca, 2013: Composite life cycle of tropical mesoscale convective systems from geostationary and low Earth orbit satellite observations: Method and sampling considerations. *Quart. J. Roy. Meteor. Soc.*, **139**, 941–953, <https://doi.org/10.1002/qj.2174>.
- Fritsch, J. M., R. J. Kane, and C. R. Chelius, 1986: The contribution of mesoscale convective weather systems to the warm-season precipitation in the united-states. *J. Climate Appl. Meteor.*, **25**, 1333–1345, [https://doi.org/10.1175/1520-0450\(1986\)025<1333:TCOMCW>2.0.CO;2](https://doi.org/10.1175/1520-0450(1986)025<1333:TCOMCW>2.0.CO;2).
- Goyens, C., D. Lauwaet, M. Schroder, M. Demuzere, and N. P. M. Van Lipzig, 2012: Tracking mesoscale convective systems in the Sahel: Relation between cloud parameters and precipitation. *Int. J. Climatol.*, **32**, 1921–1934, <https://doi.org/10.1002/joc.2407>.
- Haarsma, R. J., and Coauthors, 2016: High Resolution Model Intercomparison Project (HighResMIP v1.0) for CMIP6. *Geosci. Model Dev.*, **9**, 4185–4208, <https://doi.org/10.5194/gmd-9-4185-2016>.
- Hartmann, D. L., H. H. Hendon, and R. A. Houze, 1984: Some implications of the mesoscale circulations in tropical cloud clusters for large-scale dynamics and climate. *J. Atmos. Sci.*, **41**, 113–121, [https://doi.org/10.1175/1520-0469\(1984\)041<0113:SIOTMC>2.0.CO;2](https://doi.org/10.1175/1520-0469(1984)041<0113:SIOTMC>2.0.CO;2).
- Held, I. M., and B. J. Soden, 2006: Robust responses of the hydrological cycle to global warming. *J. Climate*, **19**, 5686–5699, <https://doi.org/10.1175/JCLI3990.1>.
- , and Coauthors, 2019: Structure and performance of GFDL's CM4.0 climate model. *J. Adv. Model. Earth Syst.*, **11**, 3691–3727, <https://doi.org/10.1029/2019MS001829>.
- Hodges, K. I., D. W. Chappell, G. J. Robinson, and G. Yang, 2000: An improved algorithm for generating global window brightness temperatures from multiple satellite infrared imagery. *J. Atmos. Oceanic Technol.*, **17**, 1296–1312, [https://doi.org/10.1175/1520-0426\(2000\)017<1296:AIAFGG>2.0.CO;2](https://doi.org/10.1175/1520-0426(2000)017<1296:AIAFGG>2.0.CO;2).
- Houze, R. A., 1989: Observed structure of mesoscale convective systems and implications for large-scale heating. *Quart. J. Roy. Meteor. Soc.*, **115**, 425–461, <https://doi.org/10.1002/qj.49711548702>.
- , 2004: Mesoscale convective systems. *Rev. Geophys.*, **42**, RG4003, <https://doi.org/10.1029/2004RG000150>.
- , 2018: 100 years of research on mesoscale convective systems. *A Century of Progress in Atmospheric and Related Sciences: Celebrating the American Meteorological Society Centennial*, *Meteor. Monogr.*, Vol. 59, 17.1–17.54, <https://doi.org/10.1175/AMSMONOGRAPHS-D-18-0001.1>.
- , K. L. Rasmussen, M. D. Zuluaga, and S. R. Brodzik, 2015: The variable nature of convection in the tropics and subtropics: A legacy of 16 years of the Tropical Rainfall Measuring Mission satellite. *Rev. Geophys.*, **53**, 994–1021, <https://doi.org/10.1002/2015RG000488>.
- Huang, X. M., C. Q. Hu, X. Huang, Y. Chu, Y. H. Tseng, G. J. Zhang, and Y. L. Lin, 2018: A long-term tropical mesoscale convective systems dataset based on a novel objective automatic tracking algorithm. *Climate Dyn.*, **51**, 3145–3159, <https://doi.org/10.1007/s00382-018-4071-0>.
- Huffman, G. J., R. F. Adler, M. M. Morrissey, D. T. Bolvin, S. Curtis, R. Joyce, B. McGavock, and J. Susskind, 2001: Global precipitation at one-degree daily resolution from multisatellite observations. *J. Hydrometeorol.*, **2**, 36–50, [https://doi.org/10.1175/1525-7541\(2001\)002<0036:GPAODD>2.0.CO;2](https://doi.org/10.1175/1525-7541(2001)002<0036:GPAODD>2.0.CO;2).
- Jeong, J. H., D. I. Lee, C. C. Wang, and I. S. Han, 2016: Characteristics of mesoscale-convective-system-produced extreme rainfall over southeastern South Korea: 7 July 2009. *Nat. Hazard Earth Syst.*, **16**, 927–939, <https://doi.org/10.5194/nhess-16-927-2016>.
- Laing, A. G., and J. M. Fritsch, 2000: The large-scale environments of the global populations of mesoscale convective complexes. *Mon. Wea. Rev.*, **128**, 2756–2776, [https://doi.org/10.1175/1520-0493\(2000\)128<2756:TLSEOT>2.0.CO;2](https://doi.org/10.1175/1520-0493(2000)128<2756:TLSEOT>2.0.CO;2).
- Lau, N. C., and M. J. Nath, 2003: Atmosphere–ocean variations in the Indo-Pacific sector during ENSO episodes. *J. Climate*, **16**, 3–20, [https://doi.org/10.1175/1520-0442\(2003\)016<0003:AOVITI>2.0.CO;2](https://doi.org/10.1175/1520-0442(2003)016<0003:AOVITI>2.0.CO;2).
- LeMone, M. A., and E. J. Zipser, 1980: Cumulonimbus vertical velocity events in GATE. Part I: Diameter, intensity and mass flux. *J. Atmos. Sci.*, **37**, 2444–2457, [https://doi.org/10.1175/1520-0469\(1980\)037<2444:CVVEIG>2.0.CO;2](https://doi.org/10.1175/1520-0469(1980)037<2444:CVVEIG>2.0.CO;2).
- Liebmann, B., and C. A. Smith, 1996: Description of a complete (interpolated) outgoing longwave radiation dataset. *Bull. Amer. Meteor. Soc.*, **77**, 1275–1277, <https://doi.org/10.1175/1520-0477-77.6.1274>.
- Lin, G. X., J. W. Fan, Z. Feng, W. I. Gustafson, P. L. Ma, and K. Zhang, 2019: Can the Multiscale Modeling Framework (MMF) simulate the MCS-associated precipitation over the central United States? *J. Adv. Model. Earth Syst.*, **11**, 4669–4686, <https://doi.org/10.1029/2019MS001849>.
- Loeb, N. G., and Coauthors, 2018: Clouds and the Earth's Radiant Energy System (CERES) Energy Balanced and Filled (EBAF) top-of-atmosphere (TOA) edition-4.0 data product. *J. Climate*, **31**, 895–918, <https://doi.org/10.1175/JCLI-D-17-0208.1>.
- Machado, L. A. T., W. B. Rossow, R. L. Guedes, and A. W. Walker, 1998: Life cycle variations of mesoscale convective systems over the Americas. *Mon. Wea. Rev.*, **126**, 1630–1654, [https://doi.org/10.1175/1520-0493\(1998\)126<1630:LCVOMC>2.0.CO;2](https://doi.org/10.1175/1520-0493(1998)126<1630:LCVOMC>2.0.CO;2).
- Mapes, B. E., and R. A. Houze, 1993: Cloud clusters and super-clusters over the oceanic warm pool. *Mon. Wea. Rev.*, **121**, 1398–1416, [https://doi.org/10.1175/1520-0493\(1993\)121<1398:CCASOT>2.0.CO;2](https://doi.org/10.1175/1520-0493(1993)121<1398:CCASOT>2.0.CO;2).
- , S. Tulich, J. Lin, and P. Zuidema, 2006: The mesoscale convection life cycle: Building block or prototype for large-scale

- tropical waves? *Dyn. Atmos. Oceans*, **42**, 3–29, <https://doi.org/10.1016/j.dynatmoce.2006.03.003>.
- McCaul, E. W., C. Cohen, and C. Kirkpatrick, 2005: The sensitivity of simulated storm structure, intensity, and precipitation efficiency to environmental temperature. *Mon. Wea. Rev.*, **133**, 3015–3037, <https://doi.org/10.1175/MWR3015.1>.
- Moncrieff, M. W., 1992: Organized convective systems: Archetypal models, mass and momentum. *Quart. J. Roy. Meteor. Soc.*, **118**, 819–850, <https://doi.org/10.1002/qj.49711850703>.
- , 2004: Analytic representation of the large-scale organization of tropical convection. *J. Atmos. Sci.*, **61**, 1521–1538, [https://doi.org/10.1175/1520-0469\(2004\)061<1521:AROTLO>2.0.CO;2](https://doi.org/10.1175/1520-0469(2004)061<1521:AROTLO>2.0.CO;2).
- , 2010: The multiscale organization of moist convection and the intersection of weather and climate. *Climate Dynamics: Why Does Climate Vary? Geophys. Monogr.*, Vol. 189, D.-Z. Sun and F. Bryan, Eds., Amer. Geophys. Union, 3–26, <https://doi.org/10.1029/2008GM000838>.
- , 2019: Toward a dynamical foundation for organized convection parameterization in GCMs. *Geophys. Res. Lett.*, **46**, 14 103–14 108, <https://doi.org/10.1029/2019GL085316>.
- , and C. Liu, 2006: Representing convective organization in prediction models by a hybrid strategy. *J. Atmos. Sci.*, **63**, 3404–3420, <https://doi.org/10.1175/JAS3812.1>.
- , D. E. Waliser, M. J. Miller, M. A. Shapiro, G. R. Asrar, and J. Caughey, 2012: Multiscale convective organization and the YOTC virtual global field campaign. *Bull. Amer. Meteor. Soc.*, **93**, 1171–1187, <https://doi.org/10.1175/BAMS-D-11-00233.1>.
- , C. H. Liu, and P. Bogenschutz, 2017: Simulation, modeling, and dynamically based parameterization of organized tropical convection for global climate models. *J. Atmos. Sci.*, **74**, 1363–1380, <https://doi.org/10.1175/JAS-D-16-0166.1>.
- Nesbitt, S. W., R. Cifelli, and S. A. Rutledge, 2006: Storm morphology and rainfall characteristics of TRMM precipitation features. *Mon. Wea. Rev.*, **134**, 2702–2721, <https://doi.org/10.1175/MWR3200.1>.
- Ohring, G., A. Gruber, and R. Ellingson, 1984: Satellite determinations of the relationship between total longwave radiation flux and infrared window radiance. *J. Climate Appl. Meteor.*, **23**, 416–425, [https://doi.org/10.1175/1520-0450\(1984\)023<0416:SDOTRB>2.0.CO;2](https://doi.org/10.1175/1520-0450(1984)023<0416:SDOTRB>2.0.CO;2).
- Parker, M. D., and R. H. Johnson, 2000: Organizational modes of midlatitude mesoscale convective systems. *Mon. Wea. Rev.*, **128**, 3413–3436, [https://doi.org/10.1175/1520-0493\(2001\)129<3413:OMOMMC>2.0.CO;2](https://doi.org/10.1175/1520-0493(2001)129<3413:OMOMMC>2.0.CO;2).
- Pope, M., C. Jakob, and M. J. Reeder, 2008: Convective systems of the north Australian monsoon. *J. Climate*, **21**, 5091–5112, <https://doi.org/10.1175/2008JCLI2304.1>.
- , —, and —, 2009: Objective classification of tropical mesoscale convective systems. *J. Climate*, **22**, 5797–5808, <https://doi.org/10.1175/2009JCLI2777.1>.
- Randall, D., C. DeMott, C. Stan, M. Khairoutdinov, J. Benedict, R. McCrary, K. Thayer-Calder, and M. Branson, 2016: Simulations of the tropical general circulation with a multiscale global model. *Multiscale Convection-Coupled Systems in the Tropics: A Tribute to Dr. Michio Yanai, Meteor. Monogr.*, Vol. **56**, Amer. Meteor. Soc., 15.1–15.15, <https://doi.org/10.1175/AMSMONOGRAPHIS-D-15-0016.1>.
- Roca, R., J. Aublanc, P. Chambon, T. Fiolleau, and N. Viltard, 2014: Robust observational quantification of the contribution of mesoscale convective systems to rainfall in the tropics. *J. Climate*, **27**, 4952–4958, <https://doi.org/10.1175/JCLI-D-13-00628.1>.
- , T. Fiolleau, and D. Bouniol, 2017: A simple model of the life cycle of mesoscale convective systems cloud shield in the tropics. *J. Climate*, **30**, 4283–4298, <https://doi.org/10.1175/JCLI-D-16-0556.1>.
- Rotunno, R., J. B. Klemp, and M. L. Weisman, 1988: A theory for strong, long-lived squall lines. *J. Atmos. Sci.*, **45**, 463–485, [https://doi.org/10.1175/1520-0469\(1988\)045<0463:ATFSL>2.0.CO;2](https://doi.org/10.1175/1520-0469(1988)045<0463:ATFSL>2.0.CO;2).
- Schumacher, R. S., and R. H. Johnson, 2006: Characteristics of U.S. extreme rain events during 1999–2003. *Wea. Forecasting*, **21**, 69–85, <https://doi.org/10.1175/WAF900.1>.
- Takemi, T., 2010: Dependence of the precipitation intensity in mesoscale convective systems to temperature lapse rate. *Atmos. Res.*, **96**, 273–285, <https://doi.org/10.1016/j.atmosres.2009.09.002>.
- Tao, W. K., and J. D. Chern, 2017: The impact of simulated mesoscale convective systems on global precipitation: A multiscale modeling study. *J. Adv. Model. Earth Syst.*, **9**, 790–809, <https://doi.org/10.1002/2016MS000836>.
- Virts, K. S., and R. A. Houze, 2015: Clouds and water vapor in the tropical tropopause transition layer over mesoscale convective systems. *J. Atmos. Sci.*, **72**, 4739–4753, <https://doi.org/10.1175/JAS-D-15-0122.1>.
- Webster, P. J., 1974: Temporal variation of low-latitude zonal circulations. *Mon. Wea. Rev.*, **101**, 803–816, [https://doi.org/10.1175/1520-0493\(1973\)101<0803:TVOLZC>2.3.CO;2](https://doi.org/10.1175/1520-0493(1973)101<0803:TVOLZC>2.3.CO;2).
- Williams, M., and R. A. Houze, 1987: Satellite-observed characteristics of winter monsoon cloud clusters. *Mon. Wea. Rev.*, **115**, 505–519, [https://doi.org/10.1175/1520-0493\(1987\)115<0505:SOCOWM>2.0.CO;2](https://doi.org/10.1175/1520-0493(1987)115<0505:SOCOWM>2.0.CO;2).
- Xing, J. L., H. Z. Ai, and S. H. Lao, 2009: Multi-object tracking through occlusions by local tracklets filtering and global tracklets association with detection responses. *Proc. IEEE Conf. Comput. Vision Pattern Recog.*, 1200–1207, <https://doi.org/10.1109/CVPR.2009.5206745>.
- Yuan, J. A., and R. A. Houze, 2010: Global variability of mesoscale convective system anvil structure from A-Train satellite data. *J. Climate*, **23**, 5864–5888, <https://doi.org/10.1175/2010JCLI3671.1>.
- Zhao, M., 2020: Simulations of atmospheric rivers, their variability and response to global warming using GFDL's new high resolution general circulation model. *J. Climate*, **33**, 10 287–10 303, <https://doi.org/10.1175/JCLI-D-20-0241.1>.
- , I. M. Held, S. J. Lin, and G. A. Vecchi, 2009: Simulations of global hurricane climatology, interannual variability, and response to global warming using a 50-km resolution GCM. *J. Climate*, **22**, 6653–6678, <https://doi.org/10.1175/2009JCLI3049.1>.
- , and Coauthors, 2018a: The GFDL global atmosphere and land model AM4.0/LM4.0: 1. Simulation characteristics with prescribed SSTs. *J. Adv. Model. Earth Syst.*, **10**, 691–734, <https://doi.org/10.1002/2017MS001208>.
- , and Coauthors, 2018b: The GFDL global atmosphere and land model AM4.0/LM4.0: 2. Model description, sensitivity studies, and tuning strategies. *J. Adv. Model. Earth Syst.*, **10**, 735–769, <https://doi.org/10.1002/2017MS001209>.